
Figures and figure supplements

Endosomal trafficking of two-pore K⁺ efflux channel TWIK2 to plasmalemma mediates NLRP3 inflammasome activation and inflammatory injury

Long Shuang Huang *et al.*

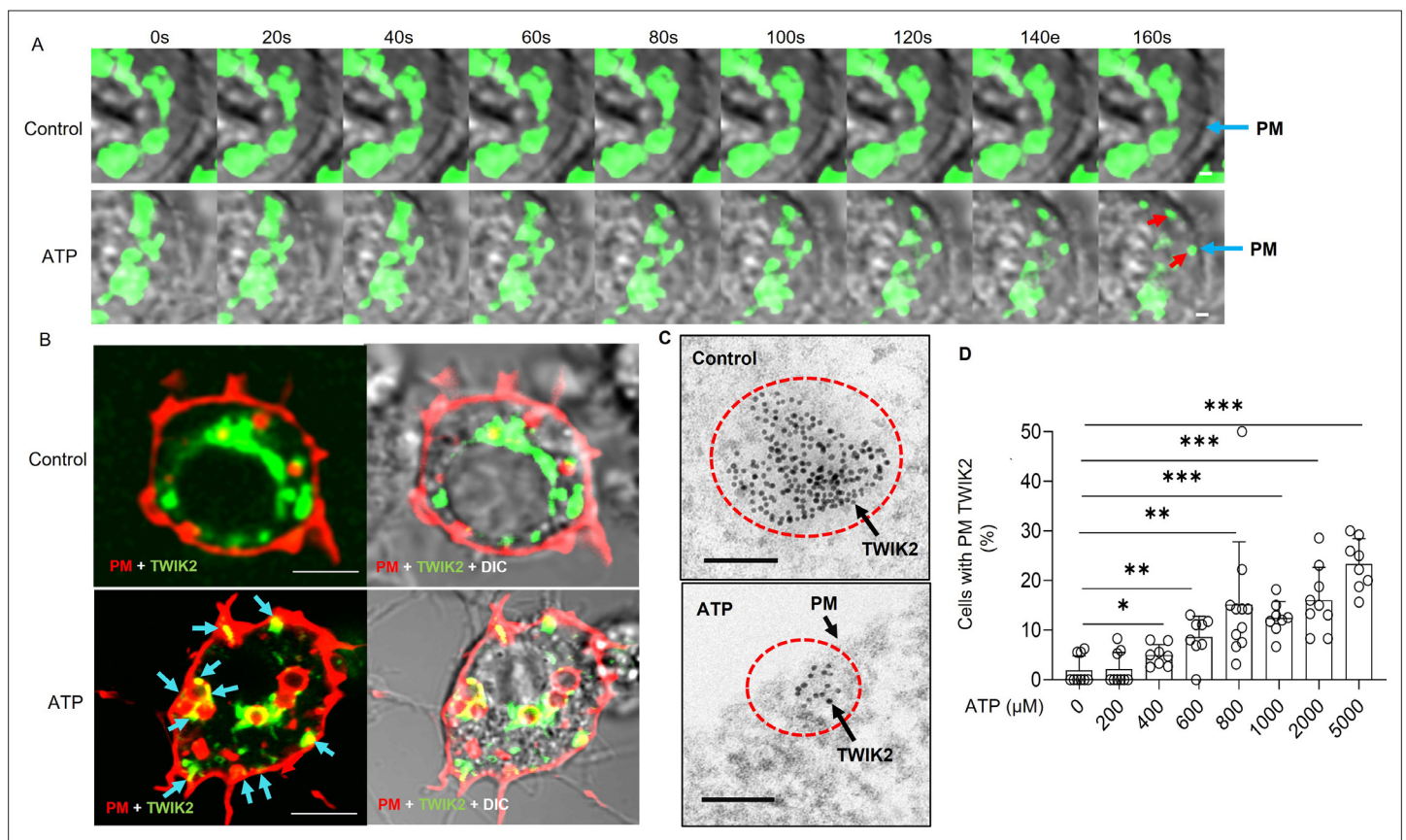


Figure 1. Intracellular TWIK2 plasmalemma translocation on ATP challenge. **(A)** Visualization of intracellular TWIK2 plasmalemma translocation post-ATP challenge. TWIK2-GFP plasmids were transfected into RAW 264.7 cells for 48 hr and cells were imaged with confocal microscope in the presence or absence of extracellular ATP (5 mM). Red arrows show translocated TWIK2 (green) on the plasma membrane (PM). Scale bar = 1 μm. **(B)** Confocal images of TWIK2 plasmalemma translocation on ATP challenge with the indicator of the plasma membrane (red) in mouse RAW 264.7 macrophage cell transfected with TWIK2-GFP plasmids (green). Cells expressing TWIK2-GFP were incubated with membrane dye NIR 750 (cell brite, #30077) for 20 m at 37°C followed by 2× wash with blank medium, stimulated with ATP or phosphate-buffered saline (PBS) (control) for 15 m; then cells were imaged using confocal microscope. Blue arrows showing the translocated TWIK2 (green) on the plasma membrane. Scale bar = 5 μm. **(C)** Confirmation of TWIK2 plasma membrane translocation using immunogold labeling electron microscopy before (upper panel) and after ATP (lower panel) (5 mM, 30 m) challenge in RAW 264.7 macrophages transfected with TWIK2 plasmids. TWIK2 (10 nm gold particles) was identified with anti-TWIK2 antibody (anti-aa71-120 of human TWIK2, Life Span Bioscience, LSBio #LS-C110195-100). Scale bar = 100 nm. Note vesicular structure outlined by immunogold marker in the upper panel and distribution of immunogold-labeled TWIK2 in the plasma membrane (PM) after ATP challenge in the lower panel. **(D)** ATP concentration-dependent TWIK2 plasma membrane translocation. TWIK2 plasma membrane (PM) translocation was analyzed using confocal images as shown in **(B)**. * $p < 0.05$, ** $p < 0.01$, *** $p < 0.001$. See also **Figure 1—figure supplement 1**.

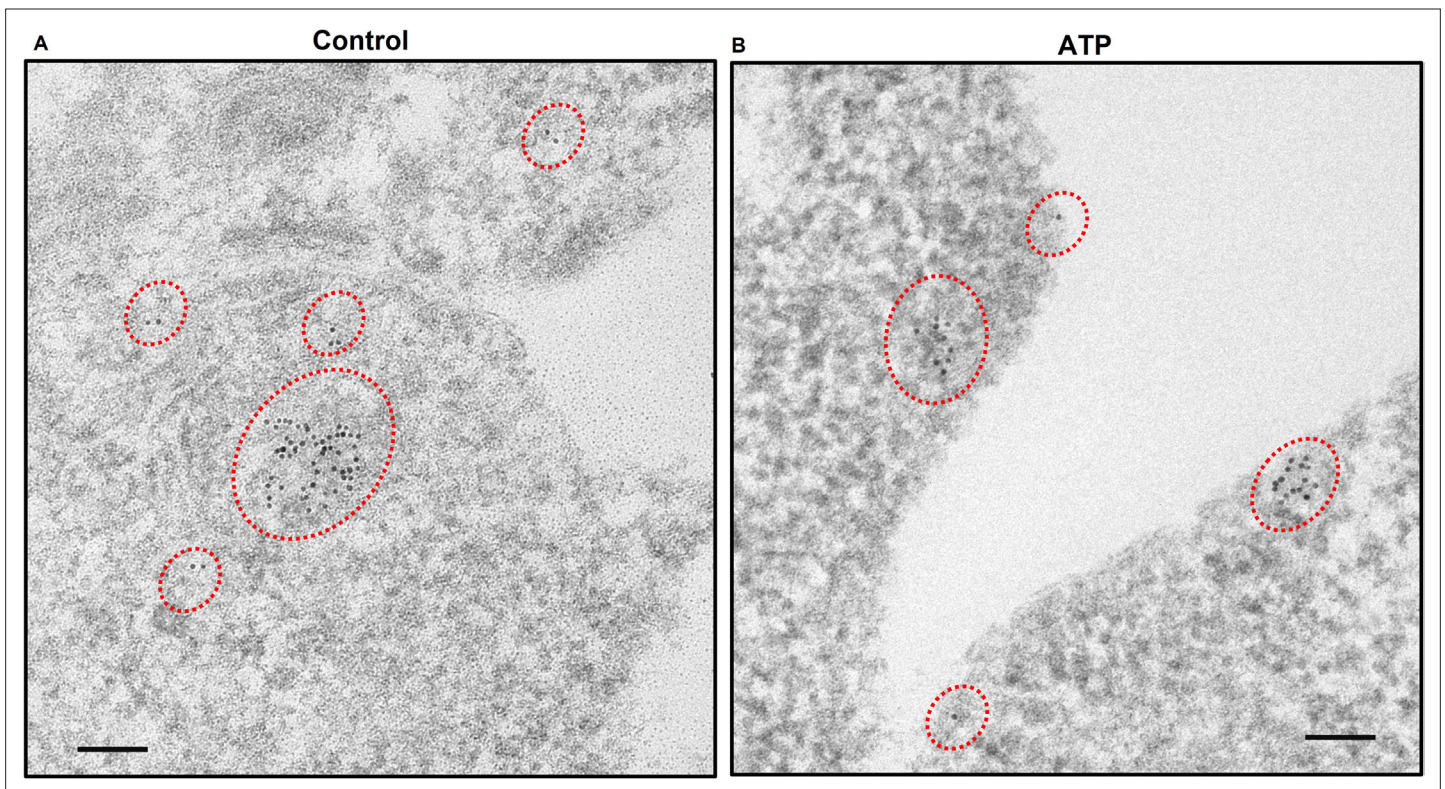


Figure 1—figure supplement 1. Electron microscopy assessment of TWIK2 plasmalemma translocation. TWIK2 plasmalemma translocation from immunogold labeling electron microscopy before (**A**) and after ATP (**B**) (5 mM, 30 min) challenge in RAW 264.7 macrophages. TWIK2 (10 nm gold particles) was identified with anti-TWIK2 antibody as in **Figure 1B**. Scale bar = 100 nm. Note the vesicular structure outlined by the immunogolds in (**A**) and plasmalemma distribution of immunogold-labeled TWIK2 after ATP challenge in (**B**). Related to **Figure 1C**.

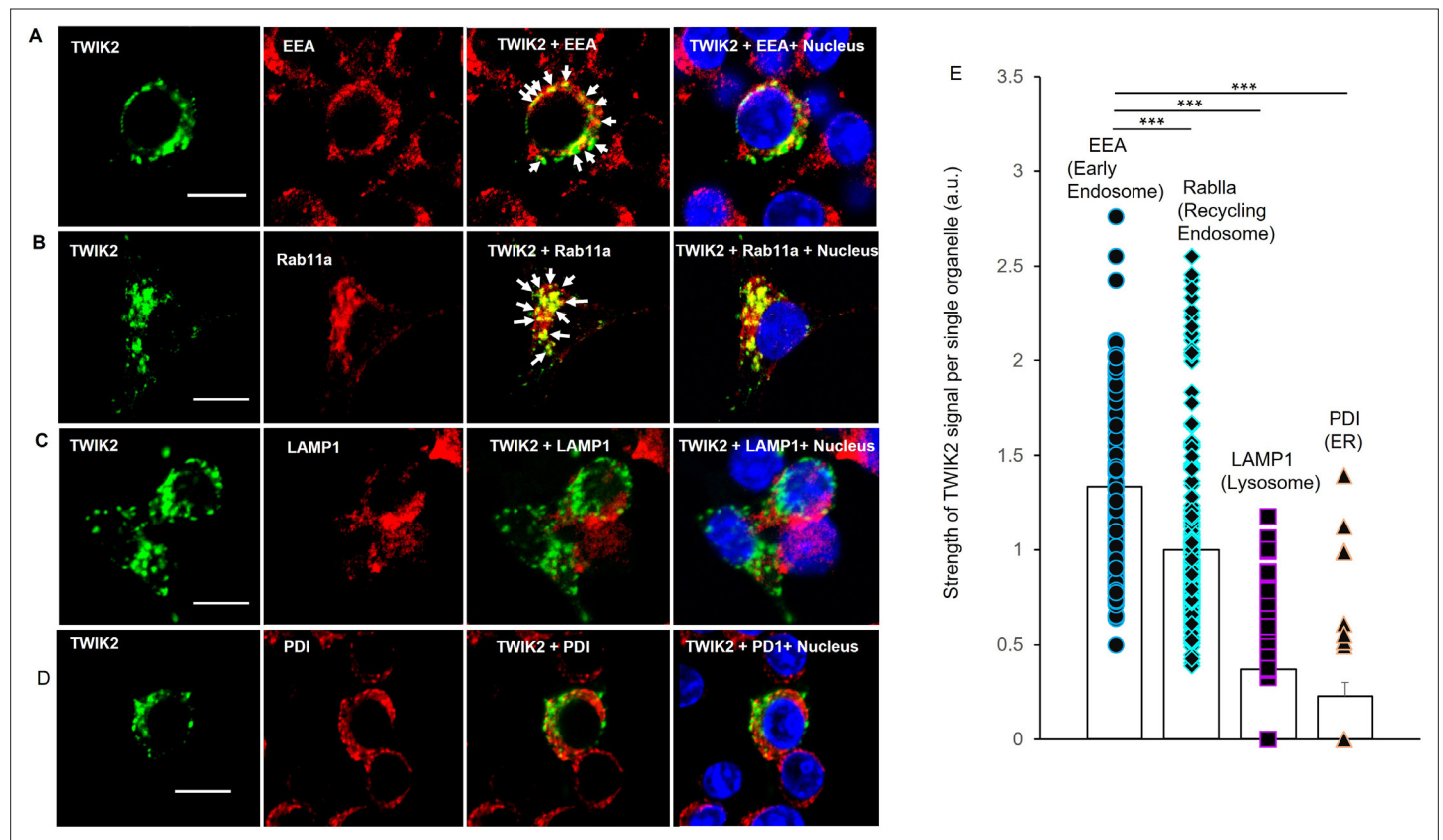


Figure 2. Endosomal localization of intracellular TWIK2 determined with fluorescent immunostaining of macrophages. TWIK2 intracellular localization was determined with fluorescent immunostaining with TWIK2 antibody along with other various antibodies against some specific vesicular proteins and imaged with confocal microscope. RAW 264.7 macrophages transfected with TWIK2 plasmids were fixed/permeabilized followed by immunostaining. TWIK2 (green) was identified with anti-TWIK2 antibody (LSBio #LS-C110195-100) in (A–D). Early endosomes (EE, red) were identified with antibody (clone1D4B) against EEA1 (C45B10 from Cell Signaling Technology) in (A). Recycling endosomes (RE, red) were identified with antibody against Rab11a (ab65200 from Abcam) in (B). Lysosomes (red) were identified with antibody against lysosomal membrane protein LAMP1 (D2D11 from Cell Signaling Technology) in (C). ER was identified with antibody against Protein Disulfide Isomerase (PDI; C81H6 from Cell Signaling Technology) in (D). Scale bar = 10 μ m. (E) Quantification of co-localization of TWIK2 with cell organelles based on the confocal images as shown in (A–D). ***p < 0.001. The localization of TWIK2 with organelles (green) was seen in both the EE and RE (white arrows) but much less in lysosomes or ER.

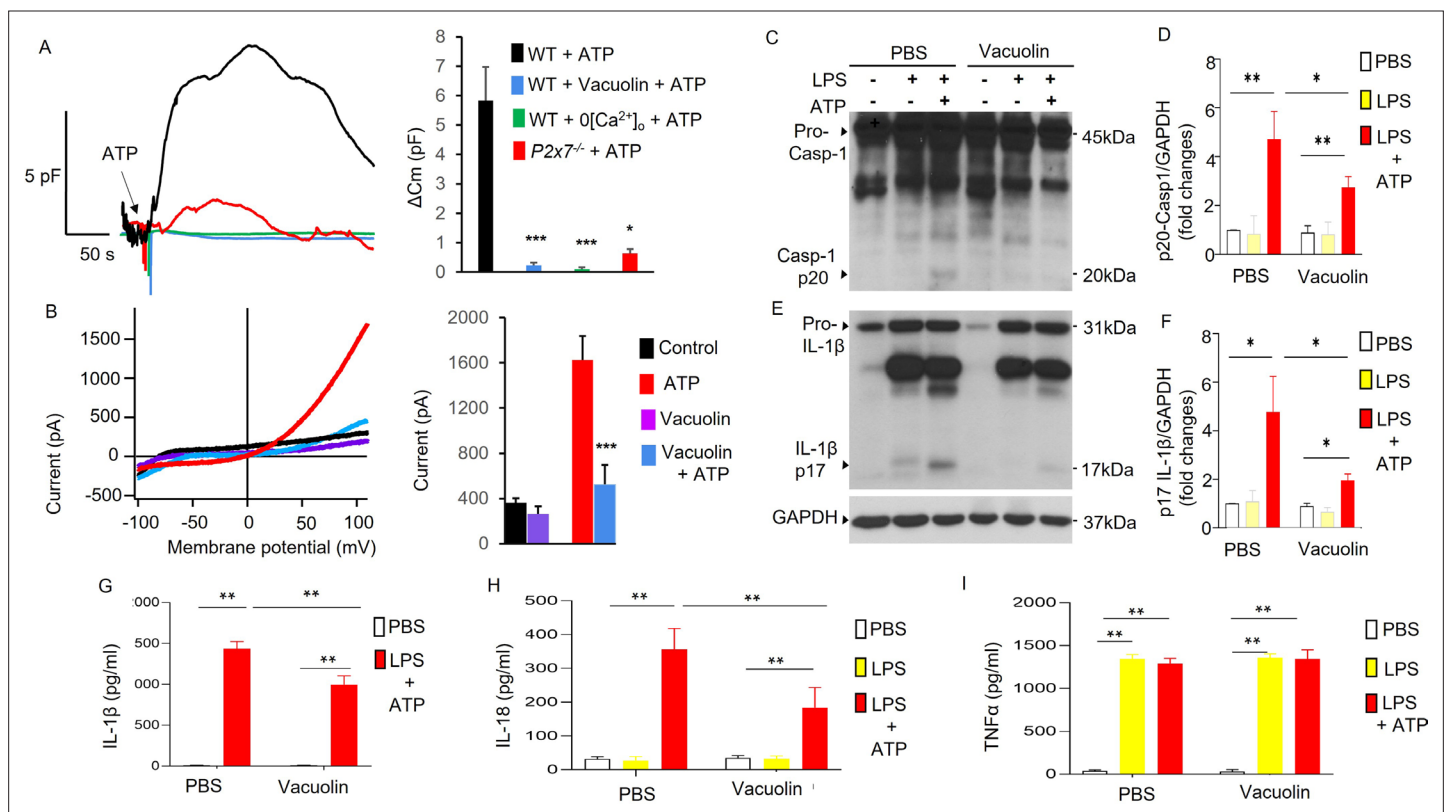
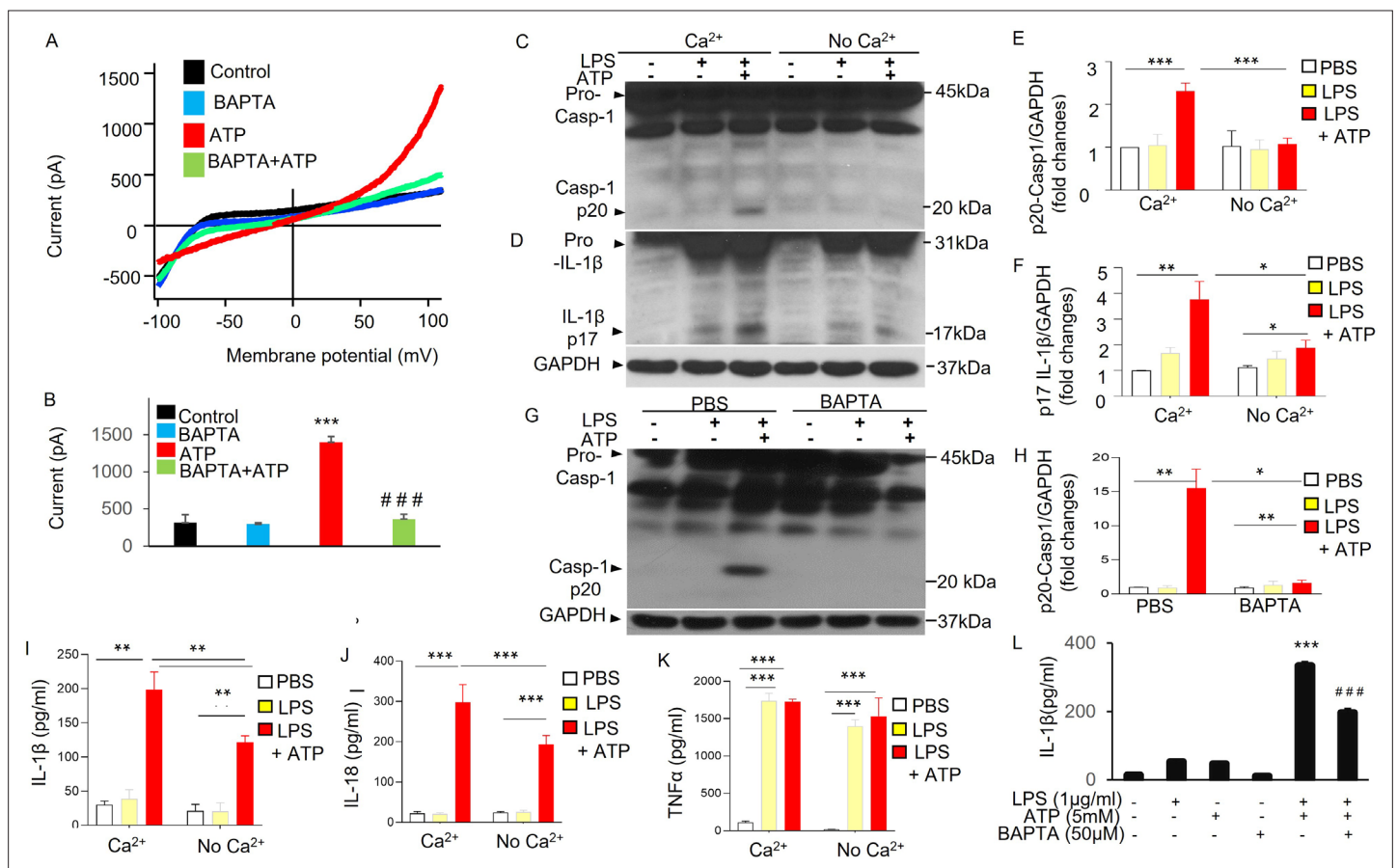


Figure 3. Association of P2X7-dependent ATP-induced exocytosis with plasmalemma potassium efflux and NLRP3 inflammasome activation. **(A, B)** Exocytic event is linked to plasmalemma potassium efflux. **(A)** Exocytosis was evaluated with measurement of whole-cell plasma membrane capacitance (Cm) reflecting the membrane surface changes. Left panel: Raw Cm traces recorded in monocyte-derived macrophages (MDMs) from either three WT or *P2x7*^{-/-} mice under different conditions: 0 extracellular Ca²⁺ (0[Ca²⁺]_o) to confirm the involvement of P2X7 which mediated Ca²⁺ influx; Vacuolin, an inhibitor of vesicle–plasma membrane fusion to confirm the involvement of membrane fusion events. 5 mM ATP was added as indicated. In the Vacuolin group, cells were treated with 10 μM Vacuolin for 2 hr before challenge with ATP. ATP treatment caused Cm increase indicating intracellular vesicle fusion with plasma membrane. Right panel: Summary of capacitance changes shown in left panel. ****p* < 0.001 compared with WT + ATP group, (*n* = 5). Vesicle–membrane fusion inhibitor Vacuolin prevented ATP-induced exocytosis (Cm increase), indicating the increased Cm caused by ATP challenge is the result of fusion of intracellular vesicles with the plasma membrane. The fusion event is both P2X7 and extracellular Ca²⁺ dependent. **(B)** Vesicle–plasmalemma fusion dependent of ATP-induced potassium efflux current. Whole-cell current was recorded with patch clamp in MDM from three mice with or without Vacuolin (10 μM). Currents were elicited with a ramp voltages running from −110 to +110 mV within 200 ms applied to cells with intervals of 1 s. Cells were held at 0 mV. Cells were bathed in solutions with K⁺ as the major outward current and Na⁺ and Ca²⁺ as the major inward current. Left panel: Representative *I*–*V* plot of whole-cell current in MDM. Right panel: Summary of experiments displayed in left panel. ****p* < 0.001 compared with ATP group (*n* = 5). Cells pretreated with the inhibitor of vesicular fusion protein Vacuolin showed significantly decreased current induced by ATP. **(C–I)** Inhibition of vesicle–plasmalemma fusion prevents NLRP3 inflammasome activation in macrophages (MDMs). Representative western blots from three independent experiments showing reduced caspase 1 activation (reduced Casp-1 p20; **C**) and IL-1β maturation (reduced IL-1β p17; **E**). MDMs from three mice pretreated with vesicle–plasmalemma fusion inhibitor Vacuolin (10 μM, 2 hr) were primed with lipopolysaccharide (LPS; 3 hr) and subsequently challenged with ATP (5 mM) for 30 min. Cell lysate was immunoblotted with indicated antibodies (anti-TWIK2 or anti-IL1β). **(D, F)** Quantification of results in **(C, E)**. **p* < 0.05, ***p* < 0.01, *n* = 3. Reduction in (Casp-1 p20) and IL-1β p17 was seen in cells treated with Vacuolin consistent with the results above. Reduction in release of IL-1β and IL-18 was also evident but TNF-α (tumor necrosis factor alpha) did not change in the presence of Vacuolin (shown in **(G, H)** and **(I)**, respectively). **p* < 0.05, ***p* < 0.01.



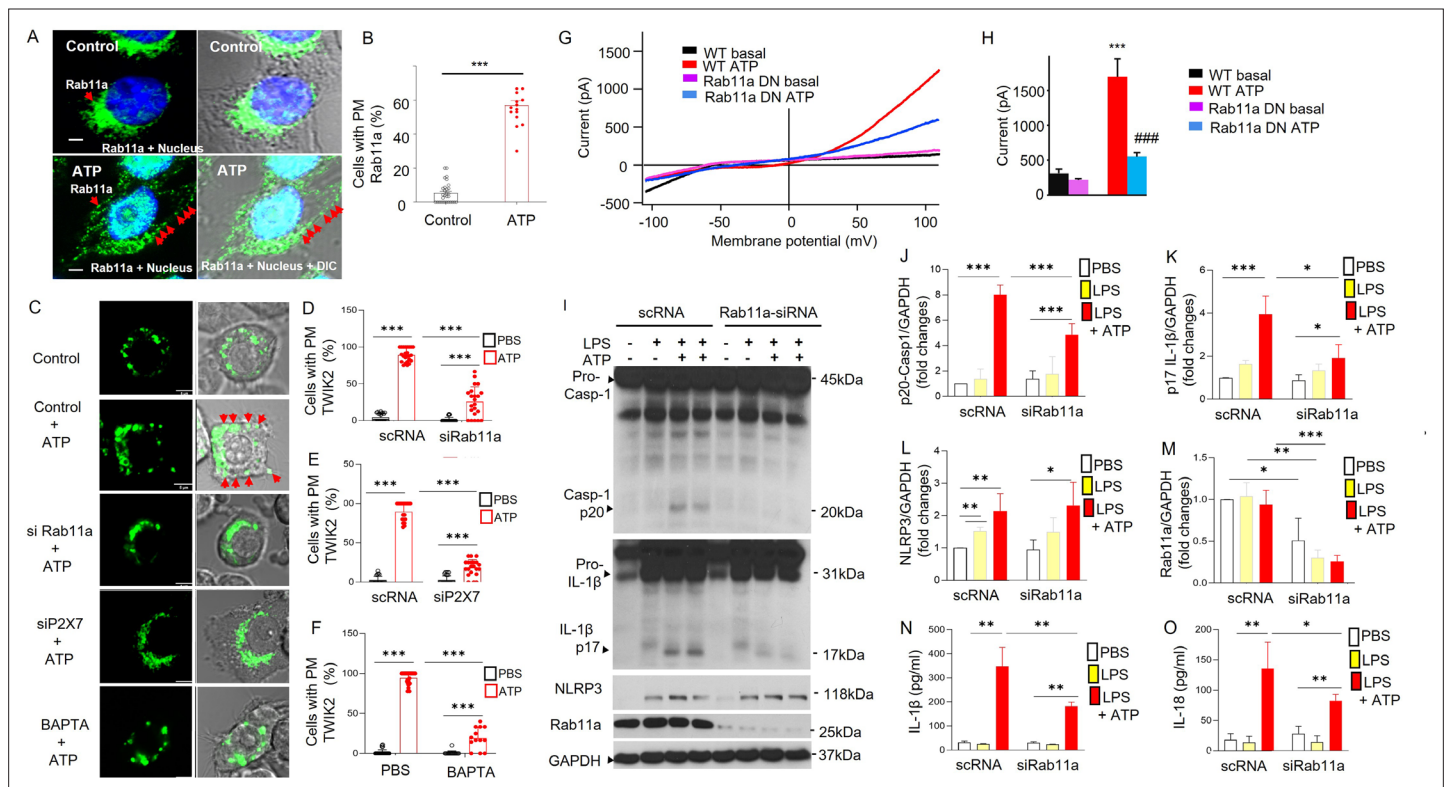


Figure 5. Rab11a mediates endosomal TWIK2 plasmalemma translocation and NLRP3 inflammasome activation on ATP challenge of macrophages. (A) Confocal images of Rab11a immunostaining in mouse monocyte-derived macrophages (MDMs) from three mice before and after ATP challenge. Rab11a (green) distribution was identified with fluorescent immunostaining with anti-Rab11a antibody (ab65200 from Abcam). Red arrows show translocated Rab11a after ATP challenge. Scale bar = 10 μ m. We observed dispersed distribution and plasmalemma translocation of Rab11a after ATP challenge (bottom panel). (B) Summary of Rab11a plasmalemma translocation as shown in (A). *** p < 0.001 compared with control group. (C–F) Rab11a-, P2X7-, and Ca^{2+} -dependent TWIK2 plasma membrane translocation induced by ATP. (C) Confocal images of TWIK2 plasmalemma translocation on ATP challenge in mouse RAW 264.7 macrophage cells transfected with TWIK2-GFP plasmids (green) under different conditions as indicated. Cells pretreated with siRab11a (or scRNA as control) or siP2X7 (or scRNA as control) for 48 hr or pretreated with BAPTA-AM (or phosphate-buffered saline [PBS] as control) for 20 m were stimulated with ATP or PBS (control) for 15 m; then the cells were imaged using a confocal microscope. Red arrows showing the translocated TWIK2 after ATP challenge. Scale bar = 5 μ m. (D–F) Quantification of the TWIK2 plasmalemma translocation under different conditions (pretreated with siRab11a (D), pretreated with siP2X7 (E), and pretreated with BAPTA-AM (F)) based on the confocal images as shown in (C). *** p < 0.001. Depletion of Rab11a or P2x7 or blocking intracellular Ca^{2+} increase (by BAPTA-AM) significantly reduced TWIK2 plasmalemma translocation after ATP challenge. (G, H) Reduced ATP-induced K^{+} outward current in RAW 264 macrophages treated with dominant-negative Rab11a (Rab11a DN) for 48 hr. Whole-cell current was recorded with patch clamp as described in Figure 3B. (G) Representative I–V plot of whole-cell current. (H) Summary from experiments displayed in (G). *** p < 0.001 compared with WT basal, n = 5. ### p < 0.001 compared with WT ATP group, n = 5. Cells pretreated with Rab11a DN showed significantly decreased current induced by ATP. (I–O) Rab11a-dependent NLRP3 inflammasome activation induced by ATP in macrophages. These experiments were carried out in MDMs treated with siRNA targeting mouse Rab11a (siRab11a). (I) Representative western blot results from three independent experiments with MDMs from three mice showing reduced caspase 1 activation (reduced Casp-1 p20), IL-1 β maturation (reduced IL-1 β p17), and depletion of Rab11a in cells treated with siRab11a in MDMs whereas NLRP3 expression was not affected by siRab11a. MDMs pretreated with siRab11a for 48 hr were primed with lipopolysaccharide (LPS; 3 hr) and subsequently challenged with ATP (5 mM) for 30 m. Cell lysates were immunoblotted with indicated antibodies (anti-TWIK2 or anti-IL1 β or anti-Rab11a or anti NLRP3). (J–M). Quantification of results shown in (I). * p < 0.05, ** p < 0.01, *** p < 0.001, n = 3. The reductions in Casp-1 p20, IL-1 β p17, Rab11a, but not NLRP3 expression were seen in cells treated with siRab11a. Reduced IL-1 β (N) and IL-18 (O) release in cells treated with siRab11a. MDMs pretreated with siRab11a for 48 hr were primed with LPS (3 hr) and subsequently challenged with ATP (5 mM) for 30 m. Release in IL-1 β and IL-18 in the supernatant was measured with ELISA. * p < 0.05, ** p < 0.01, n = 3. See also Figure 5—figure supplement 1.

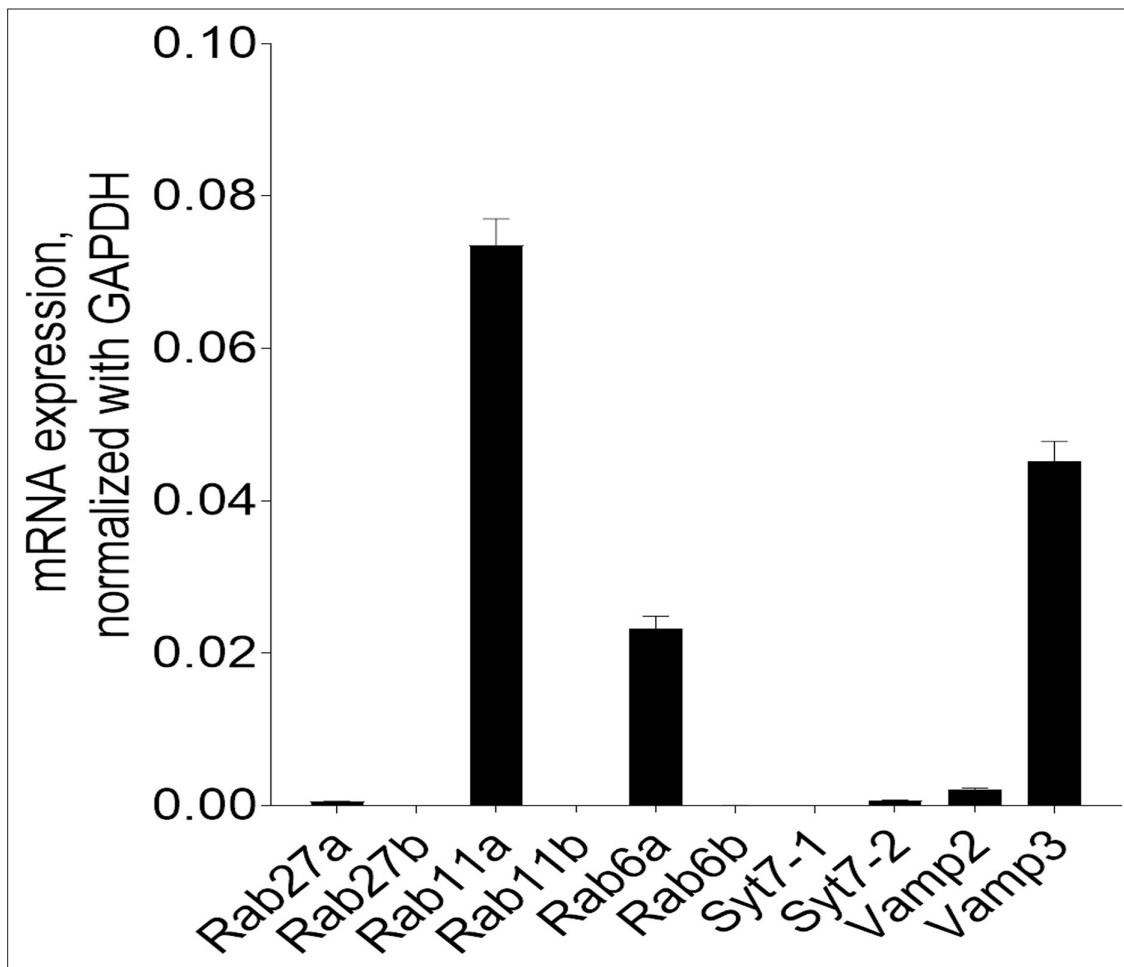


Figure 5—figure supplement 1. Relative mRNA expression of vesicle fusion proteins in monocyte-derived macrophages (MDMs). mRNA of various vesicular fusion proteins were assessed by Qrt-PCR for the following: Rab27a and b; Rab11a and b; Rab6a and b; Synaptotagmin7-1 and 2 (Syt7-1 and 2); Vamp2 and 3. The highest expression was seen in Ra11a ($n = 3$). Related to **Figure 5**.

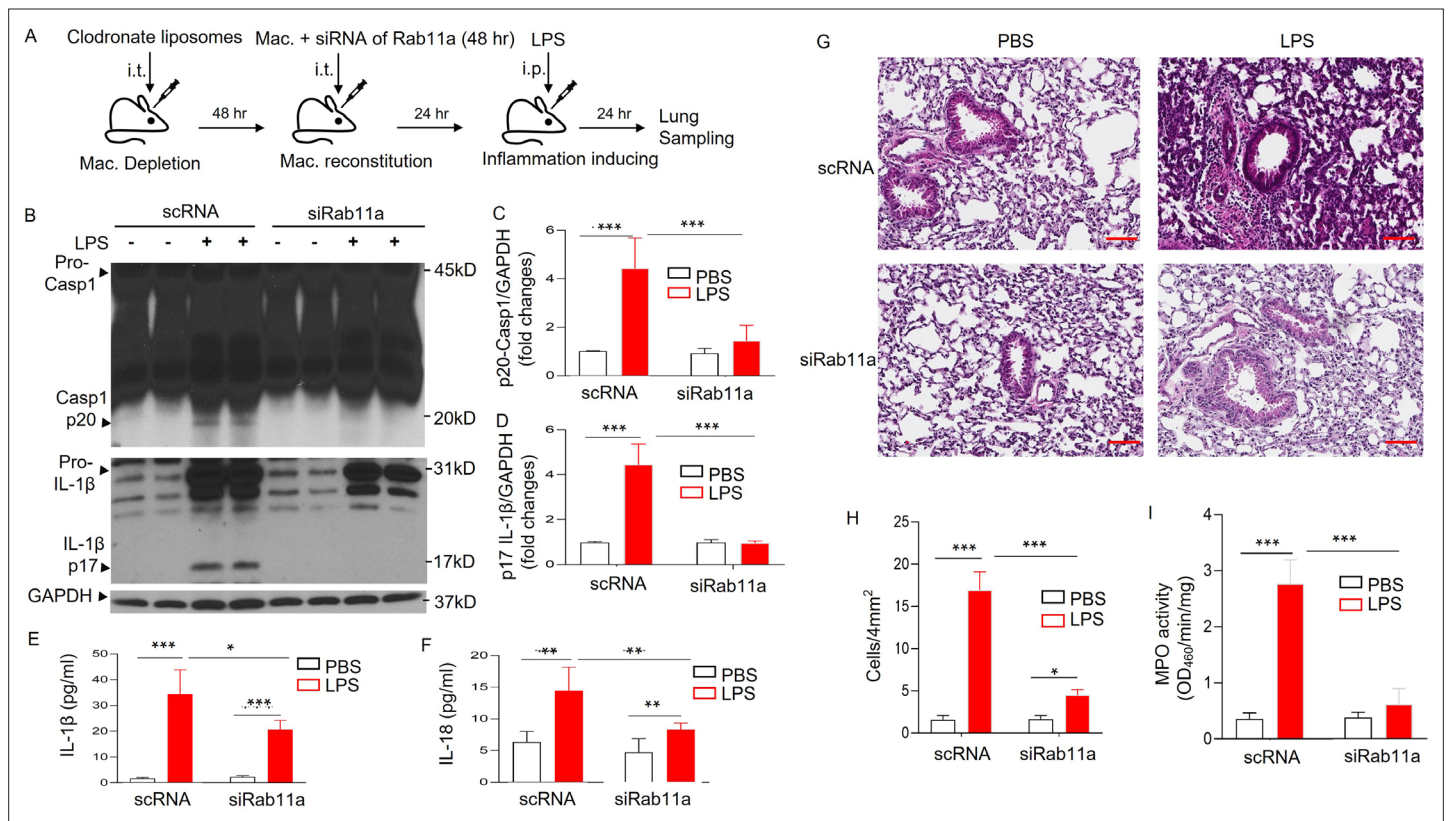


Figure 6. Rab11a deficiency in macrophages prevents sepsis-induced NLRP3 inflammasome activation and inflammatory lung injury in mice. (A) Schematic illustration of the experiments. Lung macrophages (Mac) were depleted with clodronate liposomes (for 48 hr) and then reconstituted intratracheally with monocyte-derived macrophages (MDMs) treated with either siRNA of Rab11a or scRNA control as illustrated each group (5 mice per group) were injected with lipopolysaccharide (LPS; intra-peritoneal injection, i.p.) after 24 hr of macrophage reconstitution. Lungs were harvested for evaluation of NLRP3 inflammasome activation and lung inflammation. NLRP3 inflammasome activation was evaluated by both measuring the density of Casp-1 p20 and IL-1 β p17 based on immunoblotting (B) and quantified in (C and D) (***p < 0.001, n = 5), and measuring the concentrations of IL-1 β and IL-18 shown in (E) (IL-1 β) and (F) (IL-18), *p < 0.05, **p < 0.01, ***p < 0.001, n = 5. (G) Representative H&E images of lung sections from three independent experiments (scale bars: 200 μ m). Lung injury shown in (G) was evaluated by quantification of inflammatory cells in alveoli (per 4 mm² using the Fiji image analysis software) shown in (H) (*p < 0.05, ***p < 0.001, n = 5). Lung neutrophil infiltration was evaluated by MPO measurements of lung tissue shown in (I) (***p < 0.001, n = 5). See also **Figure 6—figure supplement 1**.

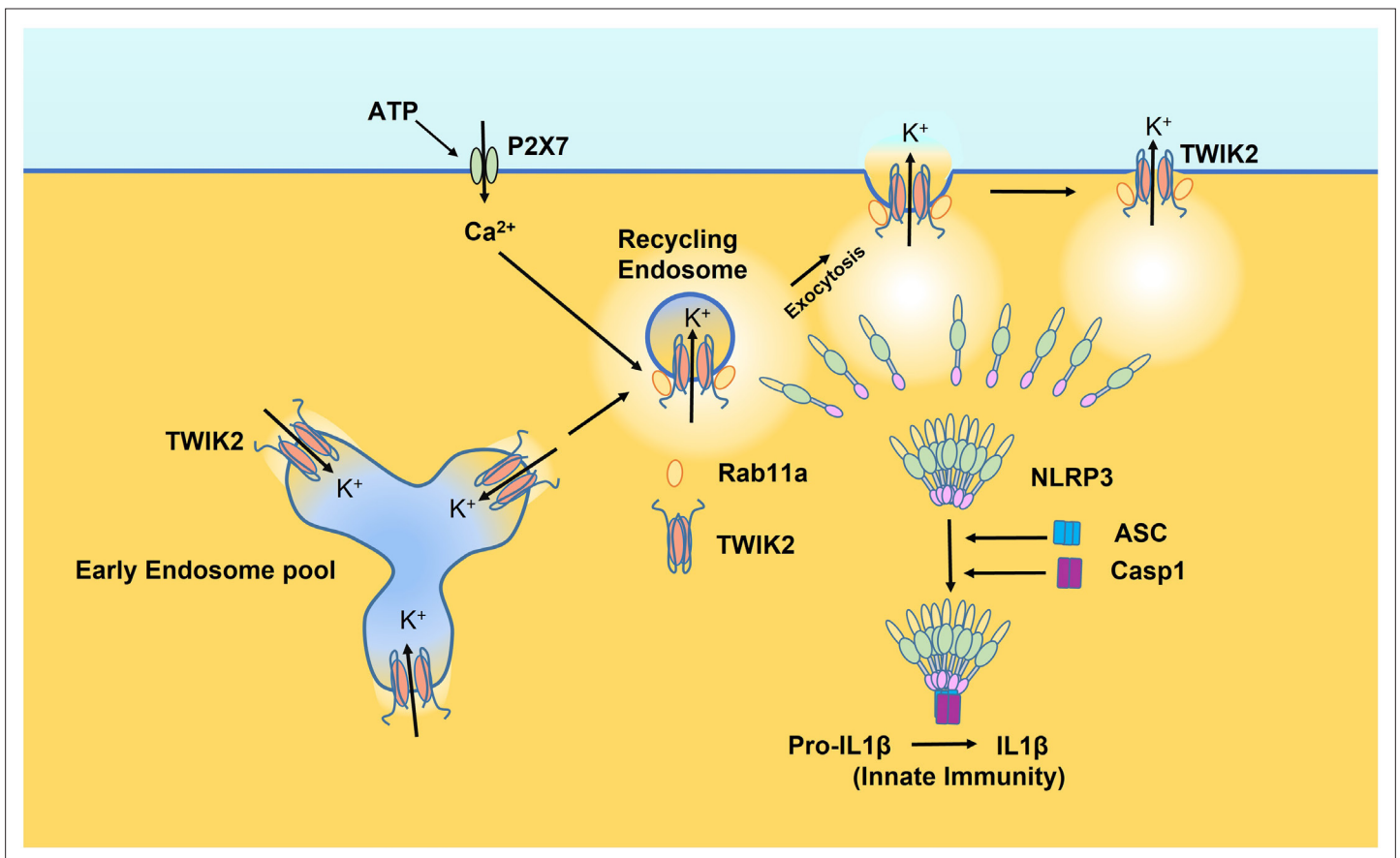


Figure 6—figure supplement 1. Endosomal TWIK2 plasmalemma translocation and resultant NLRP3 inflammasome activation. TWIK2 is basally active potassium channel in both early endosome (EE) and recycling endosome (RE). Extracellular ATP (eATP) activates P2X7 and induces Ca^{2+} influx via P2X7 which activates Ca^{2+} -sensitive Rab11a and causes recycling endosomal TWIK2 translocation to the plasma membrane. K^+ efflux via plasma membrane translocated TWIK2 causes intracellular potassium concentration ($[\text{K}^+]_{\text{in}}$) to decrease leading to NLRP3 inflammasome activation. NLRP3 inflammasome activation thus leads to macrophage activation and promotes innate immunity. Related to **Figure 6**.